An Intra-Iterative Interference Cancellation Detector for Large-Scale MIMO Communications Based on Convex Optimization

Jienan Chen, *Member, IEEE*, Zhenbing Zhang, Hao Lu, Jianhao Hu, *Member, IEEE*, and Gerald E. Sobelman, *Senior Member, IEEE*

***Abstract*—This paper proposes an intra-iterative interference cancellation (IIC) detector based on convex optimization for large-scale MIMO systems. By utilizing Newton's method to solve the optimization problem, a hardware-friendly detector is implemented in a 65 nm CMOS technology. The proposed detector has a throughput of 3.6 Gb/s with a 600 MHz operating frequency. The simulation results indicate that the block-error rate (BLER) performance of the proposed method can approach that of the minimum mean square error (MMSE) detector. The design is found to be more efficient than other recently proposed MIMO detector implementations.**

***Index Terms*—Convex optimization, intra-iterative interference cancellation, large-scale MIMO.**

I. Introduction

LARGE-SCALE multiple-input multiple-output (MIMO) systems have impressive performance characteristics, and have been selected as one of the key technologies in next-generation wireless communication systems [1]–[5]. Moreover, in [1] it is shown that, as the number of receiving antennas becomes large, the minimum mean-square error (MMSE) and zero-forcing (ZF) algorithms will approach the theoretical transmission performance limits.

On the other hand, as the number of antennas grows, the complexity of these linear processing algorithms becomes overwhelming [6]–[8]. For example, for a 128×16 MIMO system, the computational complexity of Gram matrix multiplication is on the order of 2^{15} operations. Researchers have proposed several methods to reduce the complexity of the necessary matrix inversions [9]–[12]. However, in large-scale MIMO the required matrix multiplications can be much more computationally significant than the matrix inversions, as shown in [10]. Hence, a matrix multiplication free detection method becomes attractive. A matrix multiplication free method based on the conjugate gradient method was proposed in [13]. However, the computational complexity is still relatively high for large-scale MIMO detection. The Markov chain Monte Carlo (MCMC) detection algorithm is also a matrix multiplication free method [14]–[17]. However, that detection procedure requires scanning antenna by antenna for nearly twenty iterations, which leads to a large computational load. As indicated in [18] and [19], semidefinite relaxation (SDR) optimization can also be a potential approach for MIMO detection. However, the solution method described in those works is expensive to implement in a VLSI design. The tree-searching based MIMO detection schemes such as sphere decoding and K-best decoding [22], [23] would require a high computational load if applied to large-scale MIMO systems. Hence, there remains a significant opportunity for improving the procedures for large-scale MIMO detection.

In this work, we propose an intra-iterative interference cancellation (IIC) detector for large scale MIMO systems. It is known that MIMO detection can be viewed as a convex optimization problem, which we take as our starting point. However, instead of solving the convex problem with a general-purpose CPU-based approach, we use dedicated hardware that takes advantage of the properties of the Gram matrix to reduce the computational complexity. In addition, by merging Newton's method together with MIMO detection, we obtain an implementation-friendly algorithm. To verify the performance of the proposed method, we have implemented a 128×16, 64-QAM MIMO detector in a 65 nm CMOS technology. The synthesis results indicate that the IIC detector achieves a throughput of 3.6 Gb/s with a 600 MHz operating frequency, and has a core area of 9.6 mm^2. The IIC detector avoids Gram matrix multiplication and it exhibits higher hardware efficiency (of approximately 25%), compared to existing state-of-the-art MIMO detectors. The block-error rate (BLER) performance of the fixed-point IIC has only a 0.2 dB loss compared to an MMSE detector.

The remainder of this paper is organized as follows. In Section II, we present some mathematical background and notation. The intra-iterative interference cancellation algorithm is proposed in Section III. We present the hardware implementation scheme in Section IV. The performance comparison is given in Section V, and our conclusions are presented in Section VI.

Manuscript received March 3, 2016; revised May 23, 2016 and July 9, 2016; accepted July 28, 2016. Date of publication September 9, 2016; date of current version October 25, 2016. This work was supported by National Natural Science Foundation of China under Grant 61501084 and the Fundamental Research Funds for the Central Universities A03012023601002. This paper was recommended by Associate Editor H. Johansson.

J. Chen, Z. Zhang, H. Lu, and J. Hu are with the National Key Laboratory of Science and Technology on Communications, University of Electronic Science and Technology of China, Chengdu 610054, China (e-mail: neonanme@163.com; jhhu@uestc.edu.cn).

G. E. Sobelman is with the University of Minnesota, Minneapolis, MN 55455 USA (e-mail: sobelman@umn.edu).

Color versions of one or more of the figures in this paper are available online at http://ieeexplore.ieee.org.

Digital Object Identifier 10.1109/TCSI.2016.2598060

II. Mathematical Preliminaries

A spatial-multiplexing massive MIMO system has N transmitting antennas and M receiving antennas ($M \gg N$) which can be modeled as

$$\mathbf{y} = \mathbf{H}\mathbf{s} + \mathbf{n} \tag{1}$$

where $\mathbf{H} \in \mathbb{C}^{M\times N}$ is the channel information matrix with dimension $M \times N$, $\mathbf{y} \in \mathbb{C}^M$ is a $M \times 1$ received vector, and $\mathbf{n}$ is a zero-mean Gaussian noise vector with variance σ_n^2. The transmitted symbol $\mathbf{s} \in \mathcal{O}^N$ with dimension of $N \times 1$ is mapped by a coded bit-stream, where $\mathcal{O}$ stands for the underlying complex constellation and $|\mathcal{O}| = 2^L$. Suppose a real coded bit vector $\mathbf{x}_k = [x_{k,1}\ x_{k,2}\ \cdots\ x_{k,L}]^T$ is mapped to a complex symbol $\mathbf{s}_k$ by the 2^L-QAM modulator where the b-th bit of $\mathbf{x}_k$ is denoted as $x_{k,b}$. The channel information matrix $\mathbf{H}$ is assumed to be known by the receiver. The detection of a transmitted symbol $\mathbf{s}$ can be converted to a maximum likelihood (ML) problem as

$$\mathbf{s} = \arg\min_{\mathbf{s}^\zeta \in \mathcal{O}^N} \|\mathbf{y} - \mathbf{H}\mathbf{s}^\zeta\|^2 \tag{2}$$

which has a complexity of $\mathcal{O}^N$.

A randomization approximation based on the SDR method is proposed in [18], which extracts an approximate quadratically constrained quadratic program (QCQP) solution from an SDR solution as

$$\begin{aligned} \min_{\tilde{\mathbf{s}}\in\mathbb{R}^{2N},\vartheta\in\mathbb{R}} \quad & [\tilde{\mathbf{s}}^T \quad \vartheta] \begin{bmatrix} \tilde{\mathbf{H}}^T\tilde{\mathbf{H}} & -\tilde{\mathbf{H}}^T\tilde{\mathbf{y}} \\ -\tilde{\mathbf{y}}\tilde{\mathbf{H}}^T & \|\tilde{\mathbf{y}}\|^2 \end{bmatrix} \begin{bmatrix} \tilde{\mathbf{s}} \\ \vartheta \end{bmatrix} \\ \text{s.t} \quad & \vartheta^2 = 1,\ \tilde{s}_i^2 = \left\{1, 9, \ldots \left(2^{\frac{L}{2}} - 1\right)^2\right\},\ i = 1, \ldots, 2N \end{aligned} \tag{3}$$

where

$$\tilde{\mathbf{y}} = \begin{bmatrix} \Re\{\mathbf{y}\} \\ \Im\{\mathbf{y}\} \end{bmatrix},\ \tilde{\mathbf{s}} = \begin{bmatrix} \Re\{\mathbf{s}\} \\ \Im\{\mathbf{s}\} \end{bmatrix},\ \tilde{\mathbf{H}} = \begin{bmatrix} \Re\{\mathbf{H}\} & -\Im\{\mathbf{H}\} \\ \Im\{\mathbf{H}\} & \Re\{\mathbf{H}\} \end{bmatrix}$$

in which an optimal point $\tilde{\mathbf{s}}^\star$ is solved for by the relaxed form. Then, a random feasible point is drawn from the distribution followed by $\tilde{\mathbf{s}}^\star$.

III. Intra-Iterative Interference Cancellation Detection

A. Motivation

In this work, we focus on converting traditional convex solution algorithms into a form that is feasible to implement in hardware. In contrast to previous work which solves for $\tilde{\mathbf{s}}^\star$ by transforming MIMO detection into a standard convex optimization problem, we attempt to solve for $\tilde{\mathbf{s}}^\star$ during the process of obtaining the optimal feasible point solution. In other words, the MIMO detection method is integrated together with the convex solution method.

B. Intra-Iterative Interference Cancellation Detection Based on Newton Iterations

Suppose the MIMO detection algorithm has been formulated in the form of (3), where the constraint functions are non-convex. In [18], it is suggested that the constraint functions can be relaxed or discarded. Hence, we over-relax (3) as

$$\min_{\tilde{\mathbf{s}}\in\mathbb{R}^{2N},\vartheta\in\mathbb{R}} \quad [\tilde{\mathbf{s}}^T \quad \vartheta] \begin{bmatrix} \tilde{\mathbf{H}}^T\tilde{\mathbf{H}} & -\tilde{\mathbf{H}}^T\tilde{\mathbf{y}} \\ -\tilde{\mathbf{y}}\tilde{\mathbf{H}}^T & \|\tilde{\mathbf{y}}\|^2 \end{bmatrix} \begin{bmatrix} \tilde{\mathbf{s}} \\ \vartheta \end{bmatrix} \tag{4}$$

which can be simplified back to the original ML optimization problem as

$$\min_{\tilde{\mathbf{s}}\in\mathbb{R}^{2N}} \|\tilde{\mathbf{y}} - \tilde{\mathbf{H}}\tilde{\mathbf{s}}\|^2. \tag{5}$$

Thus, the problem of (5) is an unconstrained convex optimization which can be solved by Newton's method. However, the obtained optimal point $\tilde{\mathbf{s}}^\star$ from (5) may not be a feasible point from (3). After obtaining the optimal point $\tilde{\mathbf{s}}^\star$, a set of random vectors which satisfy the constraint of (3) are generated with a followed by the distribution $\tilde{\mathbf{s}}^\star$. The detection process can be considered as sampling a suboptimal feasible signal $\tilde{\mathbf{s}}^\Theta$ from the distribution of optimal solutions, but not the feasible point $\tilde{\mathbf{s}}^\star$. Inspired by this idea, we sample the feasible data $\tilde{\mathbf{s}}^\Theta$ in the process of solving the optimization problem. Generally, solution methods for convex problems use an iterative algorithm such as Newton's method. In the process of solving for $\tilde{\mathbf{s}}^\star$, we sample the feasible data $\tilde{\mathbf{s}}^\dagger$ by the constraint function of (3). The new iteration will start at $\tilde{\mathbf{s}}^\dagger$ to approximate the optimal point. The suboptimal feasible solution $\tilde{\mathbf{s}}^\Theta$ will be obtained at the end of iteration instead of by sampling from $\tilde{\mathbf{s}}^\star$. Using this method, MIMO detection can be naturally integrated together with the convex optimization algorithm.

In this work, we employ Newton's method as the iterative solution method.

Newton's Method [21]

Given a starting point $\tilde{\mathbf{S}} \in S^{2n}$, tolerance $\varepsilon > 0$

1. Compute the Newton step and decrement $\Delta\tilde{\mathbf{S}}_{nt} := -\nabla^2 f(\tilde{\mathbf{S}})^{-1}\nabla f(\tilde{\mathbf{S}})$; $\lambda^2 = \nabla f(\tilde{\mathbf{S}})^T\nabla^2 f(\tilde{\mathbf{S}})^{-1}\nabla f(\tilde{\mathbf{S}})$
2. Line search. Choose step size ρ by backtracking line search
3. Update $\tilde{\mathbf{S}} := \tilde{\mathbf{S}} + \rho\Delta\tilde{\mathbf{S}}_{nt}$
4. Repeat 1–3 until $\lambda^2/2 \le \varepsilon$

Consider the derivation of MIMO detection based on Newton's method. The calculation of $\nabla f(\tilde{\mathbf{s}})$ and $\nabla^2 f(\tilde{\mathbf{s}})$ can be represented as

$$\begin{aligned} \nabla f(\tilde{\mathbf{s}}) &= -2\tilde{\mathbf{H}}^T\tilde{\mathbf{y}} + 2\tilde{\mathbf{H}}^T\tilde{\mathbf{H}}\tilde{\mathbf{s}} \\ \nabla^2 f(\tilde{\mathbf{s}}) &= 2(\tilde{\mathbf{H}}^T\tilde{\mathbf{H}})^T = 2\tilde{\mathbf{H}}^T\tilde{\mathbf{H}}. \end{aligned} \tag{6}$$

The Newton step is calculated by

$$\begin{aligned} \Delta\tilde{\mathbf{s}}_{nt}^{(k)} &= -\nabla^2 f(\tilde{\mathbf{s}})^{-1}\nabla f(\tilde{\mathbf{s}}) \\ &= (\tilde{\mathbf{H}}^T\tilde{\mathbf{H}})^{-1}\tilde{\mathbf{H}}^T\tilde{\mathbf{y}} - \tilde{\mathbf{s}}. \end{aligned} \tag{7}$$

If the decrement is set as $\rho = 1$, the updating of the signal is given by

$$\begin{aligned}\tilde{\mathbf{s}}^{(k+1)} &= \tilde{\mathbf{s}}^{(k)} + \Delta\tilde{\mathbf{s}}_{nt} \\ &= \tilde{\mathbf{s}}^{(k)} + \left(\tilde{\mathbf{H}}^T\tilde{\mathbf{H}}\right)^{-1}\tilde{\mathbf{H}}^T\tilde{\mathbf{y}} - \tilde{\mathbf{s}}. \end{aligned} \tag{8}$$

After multiplying on the left by $\tilde{\mathbf{H}}^T\tilde{\mathbf{H}}$, (8) can be rewritten as

$$\begin{aligned}\tilde{\mathbf{H}}^T\tilde{\mathbf{H}}\tilde{\mathbf{s}}^{(k+1)} &= \tilde{\mathbf{H}}^T\tilde{\mathbf{H}}\tilde{\mathbf{s}}^{(k)} + \tilde{\mathbf{H}}^T\tilde{\mathbf{y}} - \tilde{\mathbf{H}}^T\tilde{\mathbf{H}}\tilde{\mathbf{s}} \\ (\tilde{\mathbf{\Lambda}} + \tilde{\mathbf{V}})\tilde{\mathbf{s}}^{(k+1)} &= (\tilde{\mathbf{\Lambda}} + \tilde{\mathbf{V}})\tilde{\mathbf{s}}^{(k)} + \tilde{\mathbf{H}}^T\tilde{\mathbf{y}} - (\tilde{\mathbf{\Lambda}} + \tilde{\mathbf{V}})\tilde{\mathbf{s}} \end{aligned} \tag{9}$$

where $\tilde{\mathbf{H}}^T\tilde{\mathbf{H}} = \tilde{\mathbf{\Lambda}} + \tilde{\mathbf{V}}$. Here, $\tilde{\mathbf{\Lambda}}, \tilde{\mathbf{V}}$ denote the diagonal and off-diagonal elements of $\tilde{\mathbf{H}}^T\tilde{\mathbf{H}}$, respectively. In a large-scale MIMO system, we have $M \gg N$. Thus, the matrix $\tilde{\mathbf{H}}^T\tilde{\mathbf{H}}$ is a diagonally dominant one. Using the properties of such matrices, we obtain the following equation:

$$\left|\tilde{\mathbf{\Lambda}}\tilde{\mathbf{s}}^{(k+1)}\right|_i^2 \gg \left|\tilde{\mathbf{V}}\left(\tilde{\mathbf{s}}^{(k+1)} - \tilde{\mathbf{s}}^{(k)}\right)\right|_i^2. \tag{10}$$

Using the inequality (10), we obtain the following approximate formulation as:

$$\begin{aligned}\tilde{\mathbf{\Lambda}}\tilde{\mathbf{s}}^{(k+1)} &= \tilde{\mathbf{\Lambda}}\tilde{\mathbf{s}}^{(k)} + \tilde{\mathbf{V}}\left(\tilde{\mathbf{s}}^{(k)} - \tilde{\mathbf{s}}^{(k+1)}\right) + \tilde{\mathbf{H}}^T\tilde{\mathbf{y}} - (\tilde{\mathbf{\Lambda}} + \tilde{\mathbf{V}})\tilde{\mathbf{s}} \\ &\approx \tilde{\mathbf{\Lambda}}\tilde{\mathbf{s}}^{(k)} + \tilde{\mathbf{H}}^T\tilde{\mathbf{y}} - (\tilde{\mathbf{\Lambda}} + \tilde{\mathbf{V}})\tilde{\mathbf{s}}. \end{aligned} \tag{11}$$

For the k-th iteration, let $\tilde{\mathbf{s}} = \tilde{\mathbf{s}}^{(k)}$, and then simplify (11) as

$$\tilde{\mathbf{\Lambda}}\tilde{\mathbf{s}}^{(k+1)} \cong \tilde{\mathbf{H}}^T\tilde{\mathbf{y}} - \tilde{\mathbf{V}}\tilde{\mathbf{s}}^{(k)}. \tag{12}$$

The upshot of the formulation in (12) is that it is an iterative updating process from $\tilde{\mathbf{s}}^{(k)}$ to $\tilde{\mathbf{s}}^{(k+1)}$. For processing convenience, we convert (12) back to the complex domain and expand it in vector form as

$$\sum_{i=1}^{M} h_{ip}^* y_i - \sum_{i=1}^{M} h_{ip}^* \sum_{\substack{j=1,\\ j\neq p}}^{N} h_{ij} s_j^{(k)} = \sum_{i=1}^{M} |h_{ip}|^2 s_p^{(k+1)} \tag{13}$$

where h_{ip}^* is the conjugate form of h_{ip} in $\mathbf{H}$. The argument of the minimum function can employed to obtain $s_p^{(k+1)}$

$$s_p^{(k+1)} = \arg\min_{s_p^\zeta \in \mathcal{O}} \left(\left\| \sum_{i=1}^{M} h_{ip}^* y_i - \sum_{i=1}^{M} h_{ip}^* \sum_{\substack{j=1,\\ j\neq p}}^{N} h_{ij} s_j^{(k)} - \sum_{i=1}^{M} |h_{ip}|^2 s_p^\zeta \right\|^2 \right) \tag{14}$$

To make the notation more concise, we let λ_{SI} and λ_{SG} represent the signal interference and signal gain in (14), respectively.

$$\lambda_{\mathrm{SI}} = \sum_{i=1}^{M} h_{ip}^* \sum_{\substack{j=1,\\ j\neq p}}^{N} h_{ij} s_j^{(k)} \quad \lambda_{\mathrm{SG}} = \sum_{i=1}^{M} |h_{ip}|^2 s_p^\zeta. \tag{15}$$

In terms of signal gain, only the diagonal elements $\mathbf{\Lambda}_{pp}$ of $\mathbf{H}^H\mathbf{H}$ are required to be computed. The signal interference is calculated by

$$\sum_{i=1}^{M} h_{ip}^* \sum_{\substack{j=1,\\ j\neq k}}^{N} h_{ij} s_j^{(k)} = \left((\mathbf{H}^H\mathbf{H})\mathbf{s}^{(k)}\right)_p - \sum_{i=1}^{M} |h_{ip}|^2 s_p^{(k)}. \tag{16}$$

In (16), $\mathbf{H}^H\mathbf{H}$ is required to compute the signal interference. Using the associative law of matrix multiplication, we can rewrite the matrix multiplication in (17) as

$$\begin{aligned}(\mathbf{H}^H\mathbf{H})\mathbf{s}^{(k)} = \mathbf{H}^H\left(\mathbf{H}\cdot\mathbf{s}^{(k)}\right) = \mathbf{H}^H\cdot\mathbf{s}^\lambda \\ \mathbf{s}^\lambda = \mathbf{H}\cdot\mathbf{s}^{(k)}. \end{aligned} \tag{17}$$

In (17), only two matrix-vector multiplications are required rather than matrix multiplications, so that the complexity of the signal interference computation is reduced from $MN^2 + MN$ to $2MN$. The processing flow of IIC is summarized in Algorithm I.

Algorithm I: IIC Detection Flow

Initialize $\mathbf{s}^{(0)}$, and set the iteration time η

1. Compute the diagonal elements $\mathbf{\Lambda}$ of $\mathbf{H}^H\mathbf{H}$
2. According to $\mathbf{H}$ and $\mathbf{s}^{(k)}$, calculate the signal interference λ_{SI}
3. Cancel the signal interference as $\sum_{i=1}^{M} h_{pi}^* y_i - \lambda_{\mathrm{SI}}$
4. Search for the signal in the constellation $s_p^{(k+1)}$ by using the *argmin* function
5. Repeat step 2 to step 4, until the iteration limit η reached
6. Compute the soft LLR based on $\mathbf{s}^{(\eta)}$ and the output

It should be noted that the proposed algorithm could also operate jointly with channel decoding. The decoding bits can be remapped to $\mathbf{s}^{(k)}$ to perform the intra-iterative interference cancellation. However, we will not consider this possibility in this work.

C. Error Analysis

The detected symbol is computed by finding the nearest constellation point in (14). The successfully recovered symbols are shown as the black points in Fig. 1 falling within the constellation point circle. The points outside the circle, shown in red in Fig. 1, are mapped to error symbols. Mathematically, the conditional probability of detected symbols being inside the circle is given by

$$\begin{aligned}&\left\| \frac{\sum_{i=1}^{M} h_{ip}^* y_i - \lambda_{\mathrm{SI}}}{\sum_{i=1}^{M} |h_{ip}|^2} - s_p^{T_r} \right\| \le P_m \\ &\Rightarrow \left\| \sum_{i=1}^{M} h_{ip}^* y_i - \lambda_{\mathrm{SI}} - \sum_{i=1}^{M} |h_{ip}|^2 s_p^{T_r} \right\| \le P_m \times \sum_{i=1}^{M} |h_{ip}|^2 \end{aligned} \tag{18}$$

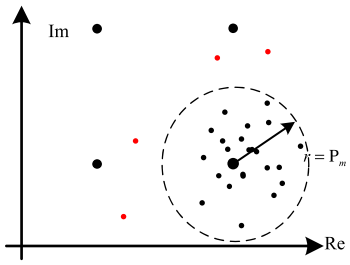

Fig. 1. Distribution of soft-detected symbols for a 64 × 8, 16-QAM MIMO system. The symbols in the circle (black dots) are correctly detected, while the symbols outside the circle (red dots) have failed to be recovered.

where $s_p^{T_r}$ is correct transmission symbol and P_m is the normalized minimal constellation power. Now, let $r = P_m$ where $\sum_{i=1}^{M} h_{ip}^* y_i$ is normalized by the signal gain $\sum_{i=1}^{M} |h_{ip}|^2$. Here, the normalized minimal constellation power P_m is denoted as

$$P_m = P_T \Bigg/ \sum_{q=1}^{2^L} s_q = P_T \Bigg/ \sum_{q=1}^{2^L} \|a + bj\|^2 \tag{19}$$

where P_T is the total transmission power. If 2^L-QAM modulation is employed in the transmitter, then an equivalent form of (19) is obtained from Appendix I as

$$P_m = P_T \Bigg/ \sqrt{4 \cdot 2^{L/2-1} \cdot \sum_{q=1}^{2^{L/2-1}} (2q-1)^2}. \tag{20}$$

We employ the arithmetic progression square summation to simplify (20) as

$$P_m = P_T \Bigg/ \sqrt{\frac{1}{3}(2^{2L} - 2^L)}. \tag{21}$$

Next, we substitute the function of signal interference into (18) to obtain

$$\left\| \sum_{i=1}^{M} h_{ip}^* \left(y_i - \sum_{\substack{j=1,\\ j\neq p}}^{N} h_{ij} s_j^{(k)} \right) - \sum_{i=1}^{M} |h_{ip}|^2 s_p^{T_r} \right\| \leq P_m \times \sum_{i=1}^{M} |h_{ip}|^2. \tag{22}$$

As indicated in (18), since $s_p^{T_r}$ is the correct transmitted symbol, the following equation holds:

$$\sum_{i=1}^{M} h_{ip}^* y_i - \sum_{i=1}^{M} |h_{ip}|^2 s_p^{T_r} = \sum_{i=1}^{M} h_{ip}^* \sum_{\substack{j=1,\\ j\neq p}}^{N} h_{ij} s_j^{T_r} + \sum_{i=1}^{M} h_{ip}^* n_i. \tag{23}$$

Substituting (23) into (22) yields the following equation:

$$\left\| \sum_{i=1}^{M} h_{ip}^* \sum_{\substack{j=1,\\ j\neq p}}^{N} h_{ij} s_j^{\Delta,(k)} + \sum_{i=1}^{M} h_{ip}^* n_i \right\| \leq P_m \times \sum_{i=1}^{M} |h_{ip}|^2 \tag{24}$$

where $s_j^{\Delta,(k)} = s_j^{T_r} - s_j^{(k)}$ can be considered as the bias estimation symbol in the k-th iteration. Note that the left-hand side of (24) is the noise-plus-interference (NPI).

We are interested in the probability distribution

$$P_s = P\left(\left\| \sum_{i=1}^{M} h_{ip}^* \left(\sum_{\substack{j=1,\\ j\neq p}}^{N} h_{ij} s_j^{\Delta,(k)} + n_i \right) \right\| \leq P_m \times \sum_{i=1}^{M} |h_{ip}|^2 \right). \tag{25}$$

On the right-hand of (22), $|h_{ip}|^2$ are the diagonal elements in $\mathbf{\Lambda}$ and $\sum_{\substack{j=1,\\ j\neq k}}^{N} \sum_{i=1}^{M} h_{ip}^* h_{ij}$ are the off-diagonal elements in $\mathbf{V}$.

$$\left\| \sum_{\substack{j=1,\\ j\neq k}}^{N} \mathbf{V}_{pj} s_j^{\Delta,(k)} + \sum_{i=1}^{M} h_{ip}^* n_i \right\| \leq P_m \times \mathbf{\Lambda}_{pp}. \tag{26}$$

The expectation of s_j in (26) is given by

$$E(\|s\|) = \sum P_s \cdot \|s\|.$$

If the transmitted symbols are evenly distributed, the expectation of s_j is equal to the average power of the transmitted symbols, given as

$$E(\|s\|) = P_A = P_T/\sqrt{2^L}. \tag{27}$$

We are interested in the ratio of P_A^2 and P_m^2 obtained from

$$K_P = P_A/P_m = \sqrt{\frac{1}{3}(2^L - 1)}. \tag{28}$$

The inequality function can be normalized by the power of the transmitted symbols as

$$\left\| K_P \cdot \sum_{\substack{j=1,\\ j\neq k}}^{N} \mathbf{V}_{pj} s_j^{\Delta,(k)} + \frac{1}{P_m} \bar{n}_k \right\| \leq \mathbf{\Lambda}_{pp} \tag{29}$$

where $\bar{n}_k = \sum_{i=1}^{M} h_{ki}^* n_i$.

The probability that the inequality (29) is satisfied is given by the following equation:

$$P_s = 1 - \int_0^{\sigma_g} f(\mathbf{\Lambda}_{pp}) d_{\mathbf{\Lambda}_{pp}} \tag{30}$$

where σ_g is the variance of left part of (29) as

$$\sigma_g = \left\| K_P \cdot \sum_{\substack{j=1,\\ j\neq k}}^{N} \mathbf{V}_{pj} s_j + \frac{1}{P_m} \bar{n}_k \right\|. \tag{31}$$

The probability density function of $\mathbf{\Lambda}_{pp}$ is given by

$$f(\mathbf{\Lambda}_{pp}) = \frac{|\mathbf{\Lambda}_{pp}|^{\frac{1}{2}(M-1)} \exp\left(-\frac{1}{2}\mathbf{\Lambda}_{pp}/\sigma_{pp}\right)}{2^{\frac{1}{2}(M-1)} \sigma_{pp}^{\frac{1}{2}(M-1)} \Gamma\left[\frac{1}{2}(M-1)\right]} \tag{32}$$

which is a χ^2 distribution with M degrees of freedom (scaled by σ_{pp}). The off-diagonal element $\mathbf{V}_{pj}$ is less familiar but can be identified as the normal variance-mean mixture where the mixing density is a χ^2 distribution [20]. The corresponding

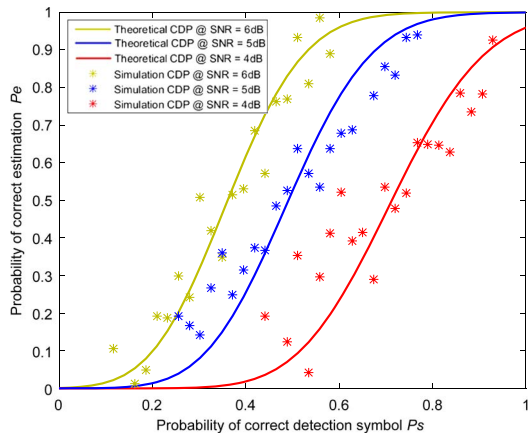

Fig. 2. Probability of correct estimation P_e at given correct detection probability P_s under different SNR with $M = 64$, $N = 8$, and 16-QAM.

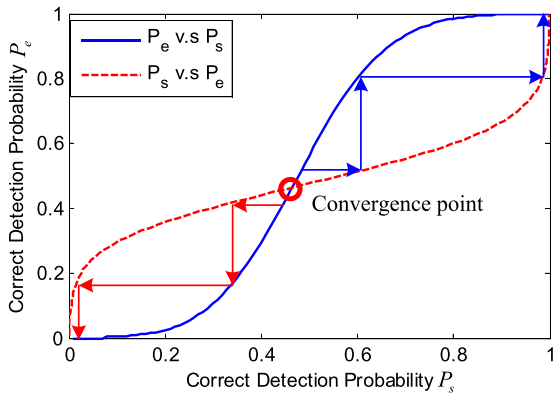

Fig. 3. The relationship between correct detection probabilities P_e and P_s.

marginal probability density for the off-diagonal element is therefore the variance-gamma distribution as

$$f(\mathbf{V}_{pj}) = \frac{|\mathbf{V}_{pj}|^{\frac{M-1}{2}}}{\Gamma\left(\frac{n}{2}\right)\sigma^{n+1}\sqrt{2^{n-1}\pi}} \cdot B_{\frac{n-1}{2}}\left(\frac{\mathbf{V}_{pj}}{\sigma^2}\right) \tag{33}$$

where $B_{n-1/2}$ is the modified Bessel function of the second kind [21]. The distribution of $\bar{n}_k$ can be approximated by $\mathbf{V}_{pi}$.

A closed-form representation of (30) can be obtain using the incomplete-Gamma function

$$F(x;k,\theta) = \int_0^x f(u;k,\theta)du = \frac{\gamma\left(k,\frac{x}{\theta}\right)}{\Gamma(k)}$$

$$F(x;k,\theta) = 1 - \sum_{i=0}^{k-1}\frac{1}{i!}\left(\frac{x}{\theta}\right)^i e^{-\frac{x}{\theta}} \tag{34}$$

Let $x = \sigma_g$ in (31) and $\theta = 2\sigma_{pp}$, the closed form expression for P_s is given by

$$P_s = \sum_{i=0}^{M-1}\frac{1}{i!}\left(\frac{K_P \cdot \sum_{\substack{j=1,\\ j\neq k}}^{N}\mathbf{V}_{pj}s_j^{\Delta,(k)} + \frac{1}{P_m}\bar{n}_k}{2\sigma_{pp}}\right)^i \times e^{-\frac{K_P\cdot\sum_{\substack{j=1,\\ j\neq k}}^{N}\mathbf{V}_{pj}s_j^{\Delta,(k)}+\frac{1}{P_m}\bar{n}_k}{2\sigma_{pp}}}. \tag{35}$$

We simulated one million random samples based on (35) to study the relationship between correct detection probability and the probability of correct detection at iteration k, P_s, where $P_e = (\sum_j^N I(s_j^{\Delta,(k)}))/N$. Here $I(s_j^{\Delta,(k)})$ is an indicator function given by

$$I\left(s_j^{\Delta,(k)}\right) = \begin{cases} 1 & \text{if } s_j^{\Delta,(k)} = 0 \\ 0 & \text{otherwise.} \end{cases}$$

Fig. 2 shows a comparison of the theoretical and simulation results for the correct detection probability (CDP) P_e at given P_s. The figure shows that the simulation and theoretical results track one another quite well, especially for the higher SNR value. We also show the convergence property of P_s and P_e in Fig. 3. If the initial P_e is above the point of convergence, the detection probability will converge at a high value, as shown by the blue path in the figure. On the other hand, if the initial P_e is below the point of convergence, the detection probability will converge at a low value, as shown by the red path in the figure. In large-scale MIMO detection, the requirement for convergence is obtained by the condition that the number of receiving antennas is much larger than the number of transmitted streams. In Fig. 4, we also depict the signal distribution in each iteration. After the third iteration, the estimated signals have converged to the correct transmitted symbols.

D. Partial Searching Method (PSM)

The new symbol is obtained by finding the minimal Euclidian distance $\min(d)$ where

$$d_k^{(\zeta)} = \left\| \sum_{i=1}^{M} h_{ip}^* y_i - \sum_{i=1}^{M} h_{ip}^* \sum_{\substack{j=1,\\ j\neq p}}^{N} h_{ij}s_j^{(k)} - \sum_{i=1}^{M}|h_{ip}|^2 s_p^{\zeta} \right\|^2 \tag{36}$$

where $s_p^{(\zeta)}$ is a 2^L-QAM constellation symbol. Then $s_p^{(k+1)}$ is achieved by finding the minimal $d_k^{(\zeta)}$ as

$$s_p^{(k+1)} = \arg\min_{s_k^{(\xi)}}\left(d_k^{(\zeta)}\right).$$

According to the above analysis, $s_p^{(k+1)}$ is distributed near the correct transmission symbol s_p^{Tr} as shown in Fig. 4. Hence we can limit our search area to nearby $s_p^{(k+1)}$ with radius r to reduce the search complexity, as shown in Fig. 5. We let $r = 1$ for 16-QAM and $r = 2$ for 64-QAM. The search symbol set is limited to

$$s_k^{(\zeta)} = \left\{ s_p^{(k)} + (a\cdot t_1 + b\cdot t_2 j) | t_1, t_2 = -r, -r+1 \cdots 0, 1, \ldots, r \right\} \tag{37}$$

where a and b are the minimal intervals in the constellation map.

The number of search points is reduced from 16 to 9 in 16-QAM, while in 64-QAM it is reduced from 64 to 25.

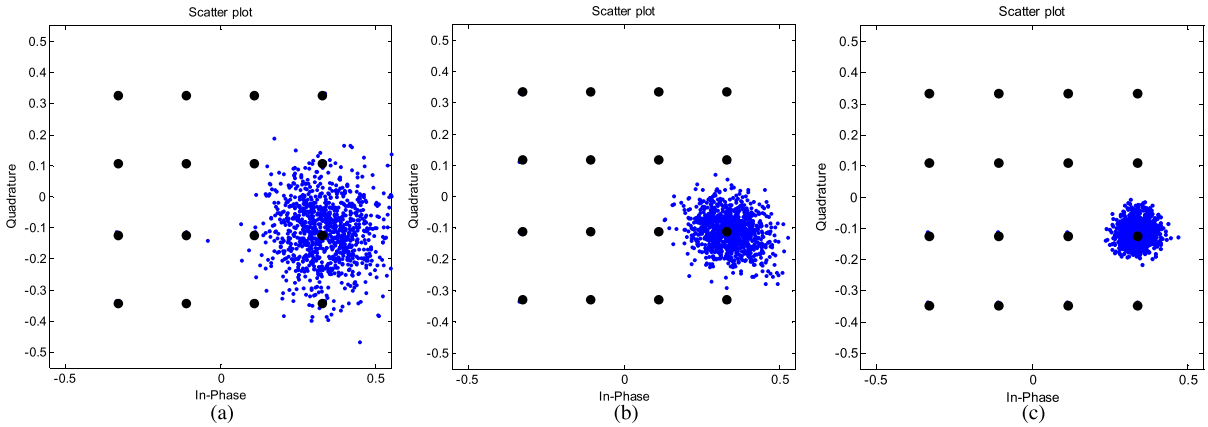

Fig. 4. The detected signal distribution in each iteration. Simulation is based on a 64 × 8, 16-QAM MIMO system, with SNR = 7 dB. (a) 1st iteration; (b) 2nd iteration; (c) 3rd iteration.

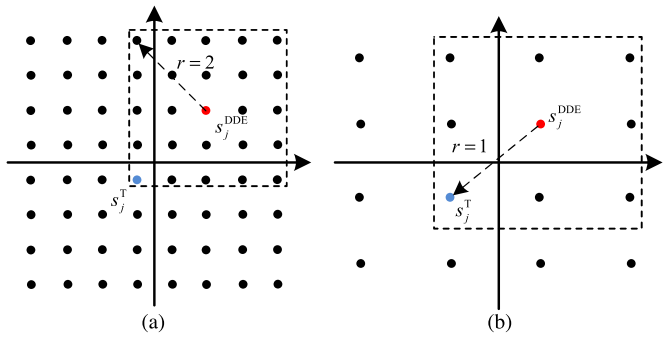

Fig. 5. The partial searching method on (a) 64-QAM and (b) 16-QAM.

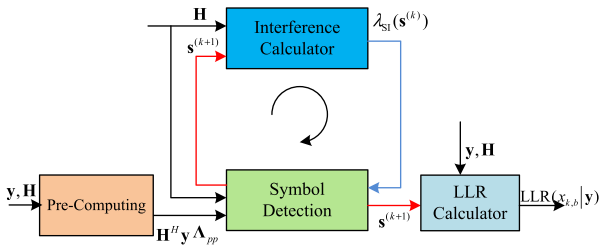

Fig. 6. High-level hardware architecture of the proposed IIC detector.

According to our simulation results, the PSM method does not lead to BLER performance loss.

IV. Hardware Architecture

The proposed IIC detector contains four main blocks, namely pre-computing, symbol detection, interference calculator, and LLR calculator, as shown in Fig. 6. In this design, the size of the MIMO system is 128 × 16 and up to a 64-QAM signal can be accommodated. The iteration limit η is set to 4. The number of computation cycles, T_s, of the proposed IIC detector is 16. Hence, the maximum throughput rate (TR) is given by

$$\mathrm{TR} = \frac{N \times L}{T_s} f_{\mathrm{clk}} = f_{\mathrm{clk}} \times 6 \tag{38}$$

where f_{clk} is the operating frequency.

A detailed description of the architecture is given in the following subsections.

A. Pre-Computing Unit

Since the IIC detector involves large-scale matrix computations, a parallel scheme is employed to accelerate the processing. The clock cycle constraint T_s is 16, and the number U_P of parallel diagonal element calculators is given by

$$U_p = N/T_s = 1. \tag{39}$$

The shadowed block diagrams in Fig. 7 indicate that the diagonal element calculators can be parallelized according to T_s and N. Similarly, the vector multiplication of $\mathbf{y}$ and $\mathbf{H}^H$ is also implemented in a U_P parallel form. Note that the multiplication schemes used in the two modules are different, requiring two or three real multipliers, respectively.

B. Interference Calculator

The main computational load in the interference calculator is given by (17). Since the iteration limit $\eta = 4$, the computation cycles of the block are restricted to $T_s/\eta = 4$. The number U_I of parallel $\mathbf{H} \cdot \mathbf{s}^{(k)}$ calculators is given by

$$U_I = \frac{M = 128}{\left(\frac{T_s}{\eta}\right) = 4} = 32. \tag{40}$$

We can normalize the constellation symbol to the axis set {1, 3, 5, 7} to reduce the computational complexity. As shown in Fig. 8, the multiplier scheme of $\mathbf{H} \cdot \mathbf{s}^{(k)}$ is implemented by three adders and two left-shifting units with a multiplexer. The same methodology was also used in [17]. The second step is the computation of $\mathbf{H}^H \cdot \mathbf{s}^{\lambda}$ which is also implemented in a $U_I = 32$ pattern.

C. Symbol Detection

After cancelling the signal interference $\lambda_{\mathrm{SI}}(\mathbf{s}^{(k)})$, the argument of the minimum operation is employed to find the $s^{\zeta} \in \mathcal{O}$ forcing the Euclidian distance of (14) to be minimal. As shown

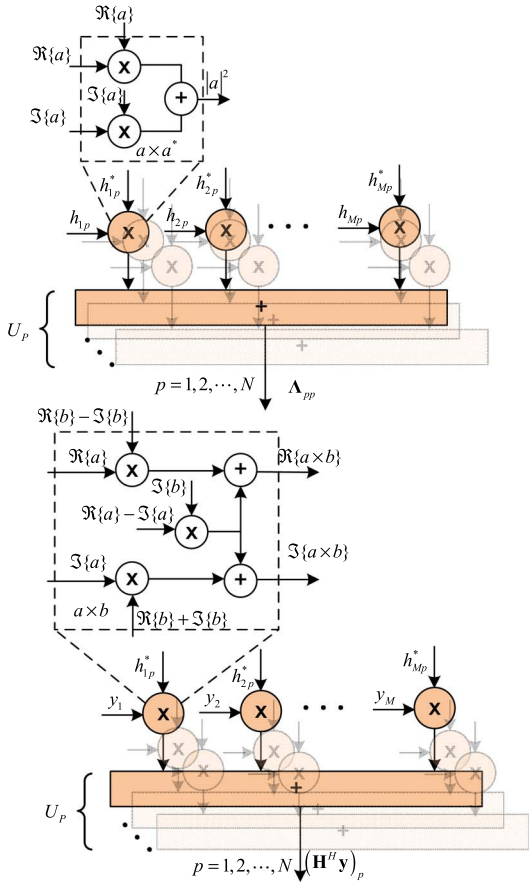

Fig. 7. Architecture of the pre-computing unit.

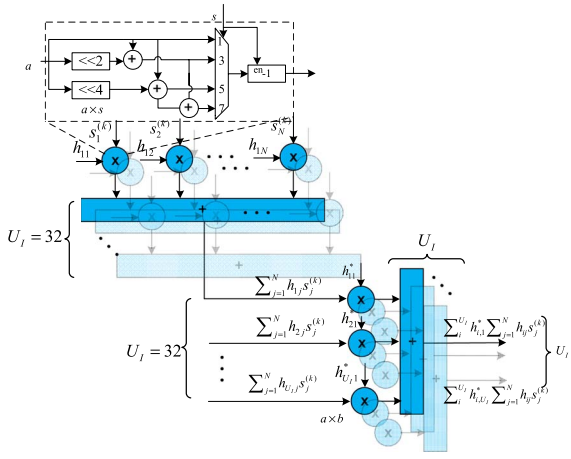

Fig. 8. Architecture of the interference calculator unit.

in Fig. 9, the diagonal element $\mathbf{\Lambda}_{pp}$ is multiplied by all constellation symbols $s_{|\mathcal{O}|}^{\dagger}$, where $|\mathcal{O}|=64$ for 64-QAM MIMO in this design. Also, the symbol detection unit is implemented in a U_{SD} parallel form, where

$$U_{SD}=\frac{N=16}{\left(\frac{T_s}{\eta}\right)=4}=4 \tag{41}$$

The detailed implementation of the LLR architecture is given in [15].

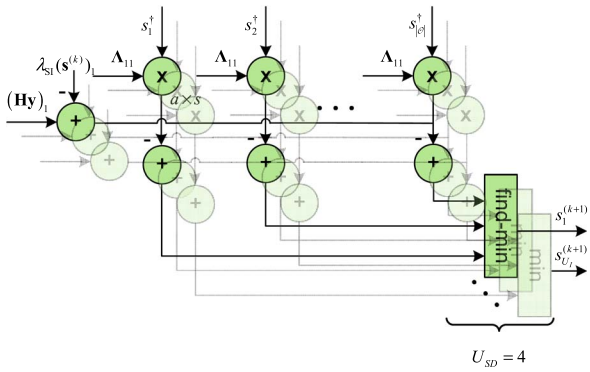

Fig. 9. Architecture of the symbol detection unit.

TABLE I
ASIC IMPLEMENTATION RESULTS FOR TWO MIMO DETECTORS. (THE DESIGN IN [11] INCLUDES AN IFFT PROCESSOR AND OTHER ADDITIONAL CIRCUITRY)

Publication	This work	M. Wu *et al.* [11]
Detection algorithm	IIC (Post Layout)	Approximated inversion
MIMO Parameter	128×16 64-QAM	128×8 64-QAM
Technology	65 nm	45 nm
MAX clock. Frequency	600 MHz	1 GHz
Throughput (Normalized Throughput)	3.6 Gbps	3.8 Gbps (2.63 Gbps)
Core Area (utilization)	9.6 mm^2 (69%)	11.1 mm^2 (73%)
Cell Area	4.3 MGE	12.6 MGE
Power consumption	1 W @ 600 Mhz	8 W @ 1 GHz

MGE: Million Gate Equivalents

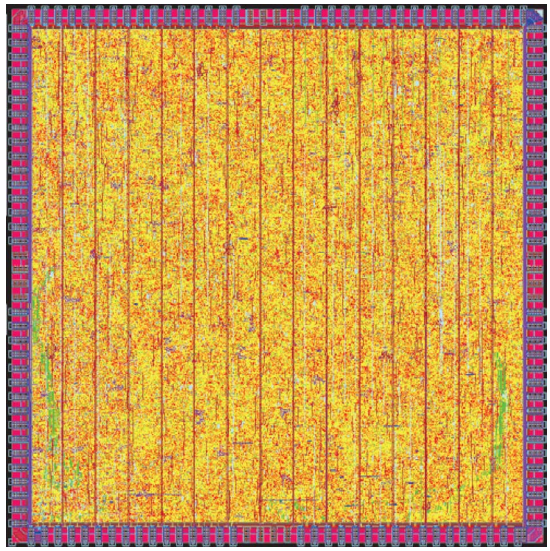

Fig. 10. Chip layout of the proposed large-scale MIMO detector.

V. IMPLEMENTATION RESULTS AND PERFORMANCE ANALYSIS

In this section, we present the hardware design metrics as well as the block error rate performance of the proposed large-scale MIMO detector.

A. Hardware Implementation Results

The ASIC implementation results are shown in Table I. The MIMO system has 128 receiving antennas and 16 transmitting

TABLE II
FPGA IMPLEMENTATION RESULTS AND COMPARISON TO OTHER REPORTED MIMO DETECTORS

Method	This work	This work	M. Wu *et al.* [10] (results from [13])	B. Yin *et al.* [13]	Studer *et al.* [7] (re-implemented and synthesized)
Detection algorithm	IIC	IIC	Approximated inversion	CGLS	MMSE (excludes the LLR input circuit)
MIMO Parameter	128×16	128×8	128×8	128×8	128×16
Slices	47 084 (30%)[a]	24123	48 244	1 094	23875
LUTs	141 252 (23%)	72231	148 797	3 324	71624
FFs	287 962 (23%)	151531	161 934	3 878	146020
DSPs	2 472 (68.6%)	1245	1 016	33	5790
Block RAM	30	16	16	1	1
Latency	67	49	196	951	117
Max Frequency	305 MHz	305 MHz	317MHz	412 MHz	300MHz
Throughput	1.83 Gb/s	915 Mb/s	621 Mb/s	20 Mb/s	900 Mb/s
Normalized Area (LUTs)[b]	1 121 k	572 k	595 k	16.4 k	1 838 k
Normalized hardware efficiency [kLUT/(Mb/s)]	0.6126	0.630	0.9581	0.8200	2.0422

[a]The percent utilization for a Virtex-7 XC7VX980T FPGA
[b]Normalized Area as given by (42)

streams with a 64-QAM signal. We synthesized the design using a 65 nm CMOS technology. The clock frequency is constrained to 600 MHz, so according to (38) the throughput is 3.6 Gbps. The chip layout of the proposed large scale MIMO detector is shown in Fig. 10. The input and output signals contain 16 bits per complex dimension. The output of a multiplier is truncated to 15 bits. The maximal width of accumulators is set to 21 bits. According to the simulation results, the performance loss of fixed-point IIC is within 0.2 dB compared to that of a floating-point design. The proposed design occupies 4.3 M gates. (It should be noted that the gate count for the detector of [11] also includes an IFFT processor and other additional circuitry.) We normalized the throughput rate (TR) of [11] to a 65 nm technology using the following equation:

$$\mathrm{TR} = \frac{M \times 2^L}{N_{\mathrm{cycle}}} f_n \quad f_n = \frac{1}{s}\, f_t$$

where N_{cycle} is number of processing cycles and f_n is the normalized frequency. Also, s is the scaling factor associated with the ASIC technologies. Here, we take $s = 65/45$ to normalize from 45 nm to 65 nm.

In order to compare with other designs in the literature, we have also synthesized our design on a Xilinx Vitex-7 XC7VX980T FPGA.

Table II provides a comparison of our IIC MIMO detector with the Neumann approximated inversion (NAI) method [10], [11], and with the conjugate gradients least square (CGLS) detector [13]. (Note that the data for the NAI design are from [13] Table I, which excludes circuitry other than the detector.) We have also re-implemented and synthesized the large-scale MMSE detector based on the algorithm proposed in [7]. For the throughput figures reported in Table II, we observe that the proposed IIC detector can achieve a processing speed up to 1.83 Gb/s, which we believe would be suitable for future 5G systems. The hardware cost is more than for NAI and CGLS detectors, but less than for an MMSE detector. The reason for this is mainly due to the larger MIMO matrix size and the more highly parallel scheme employed. The proposed MIMO detector can also be implemented in a flexible manner. For example, if we use smaller parallelization factors U_p, U_I, and U_{SD}, the hardware cost can be reduced but with a penalty of lower throughput. Alternatively, we can increase those values to obtain higher processing throughput.

As an additional, approximate measure for the overall hardware cost of the various FPGA implementations, we use the following expression for normalized area (NA):

$$\mathrm{NA} = \mathrm{LUTs} + \mathrm{DSPs} \times 280 + \mathrm{FFs}. \tag{42}$$

A 16-bit multiplier, if implemented in LUTs instead of with a DSP, would consume 280 LUTs, and we approximate that a LUT and a FF are of roughly the same order of complexity. Then, the metric of hardware efficiency in [7] is employed to compare the different schemes as

$$\mathrm{HE} = \frac{\mathrm{NA}}{\mathrm{TR}}\ (\mathrm{kLUTs/Mb/s}) \tag{43}$$

(HE: hardware efficiency, TR: throughput rate).

As can be seen from the table, the proposed method has better hardware efficiency values than the other approaches.

B. Block Error Rate Simulation

To characterize the performance of the proposed algorithm, we consider 64×8 and 128×16 MIMO systems. The channel matrices are generated using WINNER Phase II model [20]. The iteration limit of IIC is set to four. We employ a convolutional code with rate 5/6 and length 2880. A BCJR decoder with the Max-Log-MAP algorithm is used as the channel decoder. In Fig. 11, we show the BLER comparisons with the MMSE, NAI and IIC algorithms. The BLER performance of IIC approaches that of MMSE, which is believed to be near to the optimal performance for large-scale MIMO systems. For the NAI detector, it is required that the scale of receiving antennas should be much larger than the number of transmitted streams. Hence, the performance of NAI has a 1 dB performance loss when the antenna scale is 128×16. The simulation also indicates the proposed method will converge within 4 iterations.

C. Computational Complexity

Computational complexity comparisons for various detection methods are shown in Fig. 12. The number of arithmetic

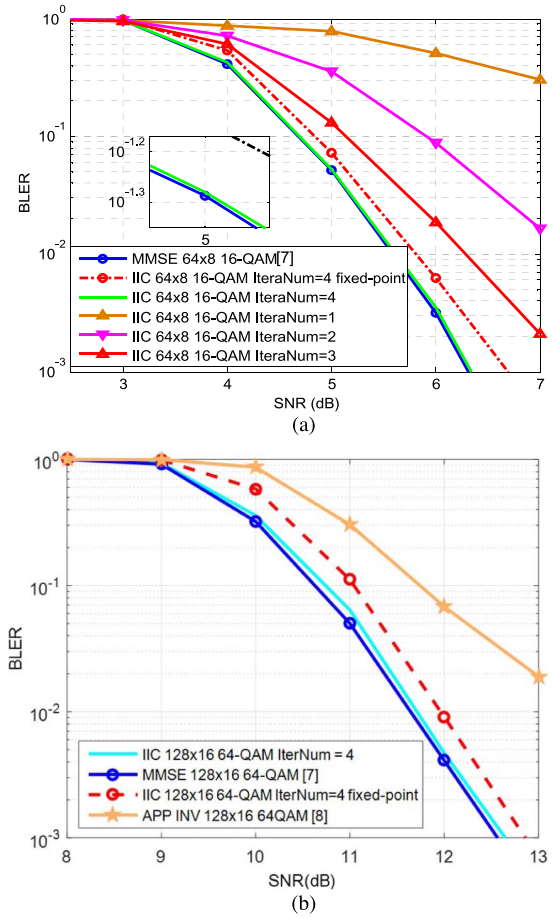

Fig. 11. BLER of large-scale MIMO system. The outer channel is a convolutional code with rate 5/6 and length 2880 and a BCJR decoder is used. (a) BLER for various 64 × 8, 16-QAM MIMO detectors. (b) BLER for various 128 × 16, 64-QAM MIMO detectors.

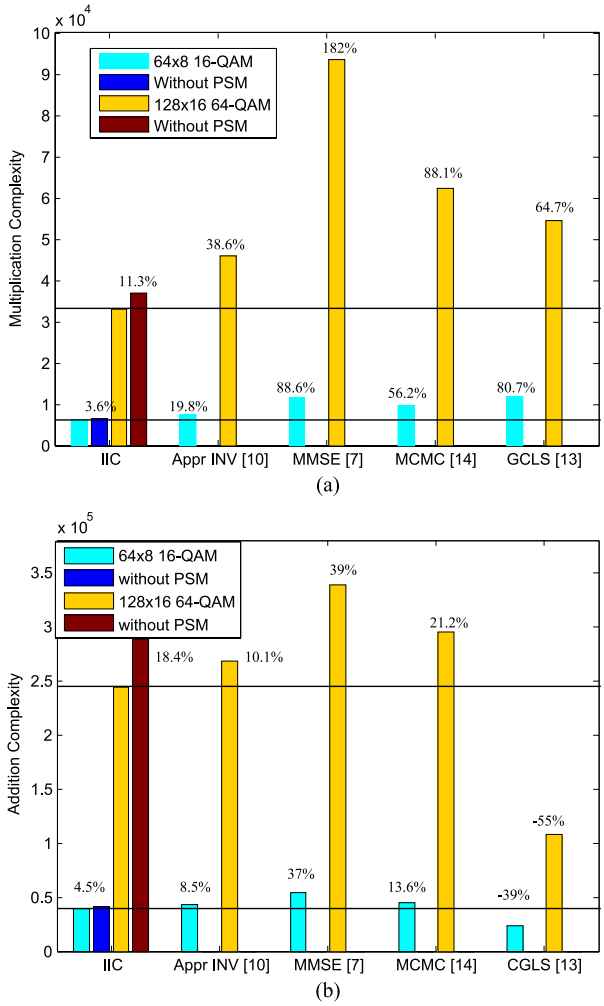

Fig. 12. Comparison of computational complexity. (a) Complexity of multiplication. (b) Complexity of addition.

operations has been calculated using the Lightspeed MATLAB toolbox.

Fig. 12(a) and (b) compare the computational complexity for massive MIMO systems of 64 × 8 16-QAM and 128 × 16 64-QAM. Since IIC requires no matrix-matrix multiplications, the number of multiplications is much lower than for existing methods. The PSM scheme also helps to reduce the complexity. The approximate inversion detector requires 38.6% more multiplications than the proposed IIC method for a 128 × 16 16-QAM MIMO detector. As the matrix dimensions grow, the IIC exhibits increased advantages compared to conventional methods. For a 128 × 16 64-QAM MIMO detector, the number of multiplications for the MMSE method is nearly twice as many as for IIC. Compared with another matrix multiplication free method, MCMC, the IIC detector requires only half the number of multiplication operations. The complexity of additions is higher than for the CGLS method proposed in [13]. However, the number of multiplications for CGLS is much higher than for the proposed method. If we approximate that a multiplication is about ten times as complex as an addition, then the overall complexity of the proposed method is about 23% less than for CGLS.

VI. Conclusion

In the work, we have proposed and implemented a novel 3.6 Gb/s Intra-Iterative Interference Cancellation detector having a high hardware efficiency for large-scale MIMO systems. Simulation results show that the block error rate performance is competitive with that of an MMSE detector, so that it would be attractive for use in the implementation of 5G systems. In our future work, we plan to consider VLSI detector architectures for situations having imperfect channel information.

Appendix I

A crucial first step in deriving the normalized minimal constellation power from (20) is to observe that

$$\min(a) = 2 \cdot \min_{i \neq j}(a_i - a_j) \quad \min(b) = 2 \cdot \min_{i \neq j}(b_i - b_j)$$

Here, we use a power metric p *to* rewrite a and b as

$$a = (2q-1)p \quad b = (2q-1)p$$

where $q = 1, 2, \ldots L$. The number of constellation points a and b are

$$N_a = N_b = \sqrt{2^L} = 2^{\frac{L}{2}}$$

Thus, the total power in one quadrant is

$$P_Q^2 = 2 \cdot \left(\frac{N_a}{2}\right) \cdot \sum_{q=1}^{N_a} P_a = 2^{\frac{L}{2}} \cdot \sum_{q=1}^{2^{L/2-1}} (2q-1)^2 p^2$$

The total power is $P_T^2 = 4P_Q^2$. The minimal power of a symbol is $(1+1)p^2$. Hence, the normalized minimal power is obtained as

$$P_m = P_T \Big/ \sqrt{4 \cdot 2^{L/2-1} \sum_{q=1}^{2^{L/2-1}} (2q-1)^2}$$

REFERENCES

[1] T. L. Marzetta, "Noncooperative cellular wireless with unlimited numbers of base station antennas," *IEEE Trans. Wireless Commun.*, vol. 9, no. 11, pp. 3590–3600, Nov. 2010.

[2] F. Rusek, D. Persson, B. K. Lau, E. G. Larsson, T. L. Marzetta, O. Edfors, and F. Tufvesson, "Scaling up MIMO: Opportunities and challenges with very large arrays," *IEEE Signal Proces. Mag.*, vol. 30, no. 1, pp. 40–46, Jan. 2013.

[3] H. Q. Ngo, E. G. Larsson, and T. L. Marzetta, "Energy and spectral efficiency of very large multiuser MIMO systems," *IEEE Trans. Commun.*, vol. 61, no. 4, pp. 1436–1449, Apr. 2013.

[4] A. Kammoun, A. Muller, E. Bjornson, and M. Debbah, "Linear precoding based on polynomial expansion: Large-scale multi-cell MIMO systems," *IEEE J. Sel. Topics Signal Process.*, vol. 8, no. 5, pp. 861–875, Oct. 2014.

[5] Y.-H. Nam, B. L. Ng, K. Sayana, Y. Li, J. Zhang, Y. Kim, and J. Lee, "Full-dimension MIMO (FD-MIMO) for next generation cellular technology," *IEEE Commun. Mag.*, vol. 51, no. 6, pp. 172–179, Jun. 2013.

[6] B. Yin, M. Wu, J. R. Cavallaro, C. Studer, "Conjugate Gradient-based Soft-Output Detection and Precoding in Massive MIMO Systems," arXiv preprint: 1404.0424v1, Apr. 2014.

[7] C. Studer, S. Fateh, and D. Seethaler, "ASIC implementation of soft-input soft-output MIMO detection using MMSE parallel interference cancellation," *IEEE J. Solid-State Circuits*, vol. 46, no. 7, pp. 1754–1765, Jul. 2011.

[8] A. Burg, S. Haene, D. Perels, P. Luethi, N. Felber, and W. Fichtner, "Algorithm and VLSI architecture for linear MMSE detection in MIMO-OFDM systems," in *Proc. IEEE International Symposium on Circuits and Systems (ISCAS)*, May 2006, pp. 4102–4105.

[9] D. Wu, J. Eilert, R. Asghar, and D. Liu, "VLSI implementation of a fixed-complexity soft-output MIMO detector for high-speed wireless," *EURASIP Journal on Wireless Communications and Networking*, vol. 2010, pp. 58:1–58:13, Apr. 2010.

[10] M. Wu, B. Yin, G. Wang, C. Dick, J. R. Cavallaro, C. Studer, "Large-scale MIMO detection for 3GPP LTE: Algorithms and FPGA implementations," *IEEE Journal of Selected Topics in Signal Processing*, vol. 8, no. 5, pp. 916–929, Oct. 2014.

[11] B. Yin, M. Wu, G. Wang, C. Dick, J. R. Cavallaro, and C. Studer, "A 3.8 Gb/s large-scale MIMO detector for 3GPP LTE-advanced," in *Proc. IEEE Int. Conf. Acoust., Speech, Signal Process. (ICASSP)*, Florence, Italy, 2014, pp. 3879–3883.

[12] B. Yin, M. Wu, C. Studer, J. R. Cavallaro, and C. Dick, "Implementation trade-offs for linear detection in large-scale MIMO systems," in *Proc. IEEE ICASSP*, May 2013, pp. 2679–2683.

[13] B. Yin, M. Wu, J. R. Cavallaro, and C. Studer, "VLSI design of large-scale soft-output MIMO detection using conjugate gradients," in *Proc. IEEE International Symposium on Circuits and Systems (ISCAS)*, May 2015, pp. 1498–1501.

[14] J. Chen, J. Hu, and G. E. Sobelman, "Stochastic Markov Chain Monte Carlo MIMO detector," *IEEE Trans. Signal Processing*, vol. 62, no. 6, pp. 1454–1463, Feb. 2014.

[15] J. Chen, J. Hu, and G. E. Sobelman, "Stochastic iterative MIMO detection system: Algorithm and hardware design," *IEEE Trans. Circuits Syst. I, Reg. Papers*, vol. 62, no. 4, pp. 1205–1214, Apr. 2015.

[16] T. Datta, N. Ashok Kumar, A. Chockalingam, and B. Sundar Rajan, "A novel MCMC algorithm for near-optimal detection in large-scale uplink mulituser MIMO systems," in *Proc. IEEE ITA*, San Diego, CA, Feb. 2012, pp. 69–77.

[17] S. A. Laraway and B. Farhang-Boroujeny, "Implementation of a Markov Chain Monte Carlo based multiuser/MIMO detector," *IEEE Trans. Circuits Syst. I, Reg. Papers*, vol. 56, no. 1, pp. 246–255, Jan. 2009.

[18] Z.-Q. Luo, W.-K. Ma, A. M.-C. So, Y. Ye and S. Zhang, "Semidefinite relaxation of quadratic optimization problems," *Signal Processing Magazine, IEEE*, vol. 27, no. 3, pp. 20–34, May 2010.

[19] W.-K. Ma, C.-C. Su, J. Jalden and C.-Y. Chi, "Some results on 16-QAM MIMO detection using semidefinite relaxation," in *Proc. IEEE Int. Conf. Acoust., Speech, Signal Process. (ICASSP)*, 2008, pp. 2673–2676.

[20] L. Hentilä, P. Kyösti, M. Käske, M. Narandzic, and M. Alatossava, Dec. 2007, Matlab Implementation of the WINNER Phase II Channel Model ver 1.1. [Online]. Available: https://www.ist-winner.org/phase2model.html

[21] S. Boyd and L. Vandenberghe, *Convex Optimization*. Cambridge, U.K.: Cambridge Univ. Press, 2004.

[22] M. Mahdavi and M. Shabany, "Novel MIMO detection algorithm for high-order constellations in the complex domain," *IEEE Trans. Very Large Scale Integration (VLSI) Systems*, vol. 21, no. 5, pp. 834–847, May 2013.

[23] C. Studer, A. Burg and H. Bolcskei, "Soft-output sphere decoding: Algorithms and VLSI implementation," *IEEE J. Sel. Areas Commun.*, vol. 26, no. 2, pp. 290–300, Feb. 2008.

Jienan Chen (S'10–M'14) received the B.S. and Ph.D degree in communication systems from the University of Electronic Science and Technology of China (UESTC), Chengdu, China in 2007 and 2014, respectively. He is currently an assistant Professor in the National Key Laboratory of Science and Technology on Communications at the UESTC.

He also worked in the School of Electrical and Computer Engineering, University of Minnesota, Minneapolis as a visiting Scholar in 2012 and 2014. His current research interests include VLSI circuit designs, low-power circuit designs, and stochastic computation based system designs.

He also worked in the School of Electrical and Computer Engineering, University of Minnesota, Minneapolis as a visiting Scholar in 2012 and 2014. His current research interests include VLSI circuit designs, low-power circuit designs, and stochastic computation based system designs.

Zhenbing Zhang received B.Sc degree in Communication Engineering from University of Electronic Science and Technology of China, Chengdu, China, in 2014. Currently he is working towards his MSc degree at the UESTC. His research interests include iterative decoding, Massive MIMO detection and Stochastic Computing.

Hao Lu received B.Sc degree in Communication Engineering from University of Electronic Science and Technology of China, Chengdu, China, in 2015. Currently he is working towards his MSc degree at the UESTC. His research interests include digital integrated circuits design and iterative decoding.

Jianhao Hu (M'10) received the B.E. and Ph.D. degrees in communication systems from the University of Electronic Science and Technology of China (UESTC) in 1993 and 1999 respectively. He joined the City University of Hong Kong from 1999 to 2000 as a postdoctoral researcher.

From 2000 to 2004, he served as a senior system engineer at the 3G research center of the University of Hong Kong. He has been a professor in the National Key Laboratory of Communication of UESTC since 2005. His research interests include high speed and low power DSP technology, VLSI, NoC, wireless communications and software radio.

Gerald E. Sobelman (M'81–SM'03) received a B.S. degree in physics from the University of California, Los Angeles. He was awarded M.S. and Ph.D. degrees in physics from Harvard University. He was a postdoctoral researcher at The Rockefeller University, and he has held senior engineering positions at Sperry Corporation and Control Data Corporation. He is currently a Professor in the Department of Electrical and Computer Engineering at the University of Minnesota. He has also served as the Director of Graduate Studies for the Graduate Program in Computer Engineering at the University of Minnesota.

Prof. Sobelman has been a Distinguished Lecturer of the IEEE Circuits and Systems Society, and he has served on the technical program committees for IEEE ISCAS, IEEE SOCC and IEEE ICCSC. He was Chair of the Technical Committee on Circuits and Systems for Communications of the IEEE Circuits and Systems Society, and he has also served as an Associate Editor for IEEE TRANSACTIONS ON CIRCUITS AND SYSTEMS I and for IEEE SIGNAL PROCESSING LETTERS. He was Local Arrangements Chair for the 1993 IEEE International Conference on Acoustics, Speech and Signal Processing. In addition, he has chaired many sessions at international conferences in the areas of communications and VLSI design. He has developed and presented short courses on digital VLSI design at several industrial sites. His current research interests are in the areas of VLSI circuit and system design for applications in communications and signal processing.